Photoacoustics 37 (2024) 100599

Contents lists available at ScienceDirect

Photoacoustics

journal homepage: www.elsevier.com/locate/pacs

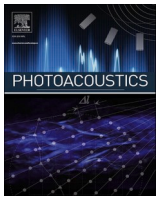

No document header

Study of erythrocyte sedimentation in human blood through the photoacoustic signals analysis

Argelia Pérez-Pacheco [a,*,1], Roberto G. Ramírez-Chavarría [b,**], Marco Polo Colín-García [c], Flor del Carmen Cortés-Ortegón [c], Rosa María Quispe-Siccha [a], Adolfo Martínez-Tovar [d], Irma Olarte-Carrillo [d], Luis Polo-Parada [e], Gerardo Gutiérrez-Juárez [f]

[a] Unidad de Investigación y Desarrollo Tecnológico (UIDT), Hospital General de México, Dr. Eduardo Liceaga, Ciudad de México 06726, Mexico
[b] Instituto de Ingeniería, Universidad Nacional Autónoma de México, Ciudad de México 04510, Mexico
[c] Instituto de Ciencias Aplicadas y Tecnología (ICAT), Universidad Nacional Autónoma de México, Apartado Postal 70-186, Ciudad de México 04510, Mexico
[d] Laboratorio de Biología Molecular, Servicio de Hematología, Hospital General de México, Dr. Eduardo Liceaga, Ciudad de México 06726, Mexico
[e] Department of Medical Pharmacology and Physiology and Dalton Cardiovascular Research Center, University of Missouri, Columbia, MO 65211, USA
[f] Departamento de Ingeniería Física, División de Ciencias e Ingenierías, Universidad de Guanajuato-Campus León, León, Guanajuato C.P. 37150, Mexico

ARTICLE INFO

Keywords:
Whole human blood
Aggregation
Erythrocyte sedimentation
Anemia
Speed of sound
Pulsed photoacoustic

ABSTRACT

Introduction: In this study, we utilized the pulsed photoacoustic (PA) technique to analyze globular sedimentation in whole human blood, with a focus on distinguishing between healthy individuals and those with hemolytic anemia.
Methods: Blood samples were collected from both healthy individuals (women and men) and those with hemolytic anemia, and temporal and spectral parameters of PA signals were employed for analysis.
Results: Significant differences ($p < 0.05$) were observed in PA metrics between the two groups. The proposed spectral analysis allowed significant differentiation within a 25-minute measurement window. Anemic blood samples exhibited higher erythrocyte sedimentation rate (ESR) values, indicating increased erythrocyte aggregation.
Discussion: This study underscores the potential of PA signal analysis in ESR assessment as an efficient method for distinguishing between healthy and anemic blood, surpassing traditional approaches. It represents a promising contribution to the development of precise and sensitive techniques for analyzing human blood samples in clinical settings.

1. Introduction

The Erythrocyte Sedimentation Rate (ESR) is a hematological test first described over 120 years ago, considered a marker of inflammation and a strong predictor of coronary heart disease mortality [1–3]. An increase in ESR is associated mainly with inflammatory, neoplastic problems, or anemias, whereas a decrease is related to congenital erythrocyte alterations, polycythemia, and heart failure [4,5]. To date, the Westergren method is considered "the gold standard" for determining the ESR, recognized by the International Council (previously Committee) for Standardization in Haematology (ICSH) [6,7]. This method measures the distance in millimeters that red blood cells (RBCs) travel in one hour as they descend to the bottom of a vertical column. The Westergren method uses an anticoagulant that can be liquid-based (citrate) or solid-based (ethylenediaminetetraacetic acid, EDTA). Citrate results in the dilution of blood, inaccuracies of which significantly affect the ESR. The ESR values obtained by the Westergren method are nonspecific; they are subject to various errors due to technical factors or RBCs size, shape, and concentration. Typically, normal RBCs cluster together in a line or roll shape, like a stack of coins, a process known as *Rouleaux* [8]. In contrast, abnormal RBCs may cluster irregularly due to various factors like changes in sialic acid levels in the cell membrane,

* Correspondence to: Researcher in Medical Sciences, Research and Technological Development Unit (UIDT), Hospital General de México "Dr. Eduardo Liceaga", Dr. Balmis 148, Doctores, Ciudad de Mexico, Cuauhtémoc C.P. 06726., Mexico
** Correspondence to: Electro-Mechanics Department at Instituto de Ingeniería, Universidad Nacional Autónoma de México, Ciudad de México 04510, Mexico.
E-mail addresses: argeliapp@ciencias.unam.mx (A. Pérez-Pacheco), RRamirezC@iingen.unam.mx (R.G. Ramírez-Chavarría).
[1] https://orcid.org/0000-0002-5261-1482

https://doi.org/10.1016/j.pacs.2024.100599
Received 3 October 2023; Received in revised form 22 December 2023; Accepted 26 February 2024
Available online 2 March 2024

temperature, pH, viscosity, osmolarity, and the ionic strength of their surrounding fluid [9]. These changes can either increase or decrease the ESR. For instance, anemia can lead to more rouleaux formation, while polycythemia reduces it [10,11]. RBCs aggregation significantly impacts ESR, but the underlying mechanisms are not completely understood [12]. The ESR process involves three stages: aggregation, sedimentation, and packing of RBCs [13].

New automated and non-automated methods have been proposed for the measurement of ESR; however, these are limited by one or more of the following factors: time-consuming preparation procedures, costly systems, low sensitivity, technical errors, single parameter measurement or alteration in samples due to light scattering and/or transmission [14–17].

In recent decades, PA techniques have gained wide acceptance in the biomedical community because they combine the high sensitivity of optical absorbance and the high resolution of ultrasound, as well as being safe since there is no ionizing radiation involved in most cases [18,19]. The pulsed PA technique is based on the absorption of short-pulsed light and volume expansion of the irradiated sample, generating acoustic waves at megahertz (MHz) frequencies. Among a broad range of applications, the PA technique has been used to detect and monitor RBCs sedimentation and aggregation, providing information on their oxygenation levels [20–29]. Various experimental setups have been proposed using different fluences, wavelengths, ultrasound sensors, and synthetic materials. However, these studies have mainly focused on the study of animal blood [20,21,25,30–32] or human blood extracted from a single donor [20,33–35], which were diluted with PBS and/or inducing sedimentation and aggregation with dextran [23,24]. Theoretical and experimental models based on suspended particles have also been carried out using the PA technique, using different synthetic materials that are not ordinarily present in blood samples [22,26,36–39]. Therefore, the results of these studies are not conclusive regarding the ESR and cannot be easily extended to human blood samples or those with specific pathologies (Table 1. General experimental characteristics of published studies related to ESR and/or RBCs aggregation in blood samples using the PA technique).

In this work, we have developed an experimental system that enables the acquisition of PA signals from blood samples collected from individuals diagnosed with hemolytic anemia and healthy subjects. The PA signals were analyzed to extract various parameters before, during, and after globular sedimentation. Our findings revealed significant statistical differences across all the PA variables analyzed between anemic and healthy blood. Furthermore, we introduced a new and innovative analysis of spectral parameters of the signals within the initial minutes of the sedimentation process, facilitating rapid differentiation between blood samples with and without anemia when compared to conventional techniques (e.g., Wintrobe and Westergren methods), yielding a high P-value. Our system operates without the need for any chemicals or solutions, eliminating the requirement for inducing aggregation in the sample, such as dextran or any dilution. The laser beam, responsible for generating the photoacoustic signal, was oriented perpendicularly to the sedimentation direction, as opposed to parallel. This design choice prevented optical saturation and allowed for the detection of photoacoustic sources (erythrocytes) throughout the sedimentation process. Moreover, no lens was required to focus the laser beam and the fluence was well below those reported in earlier research [24,30,38].

1.1. Hemolytic anemia and erythrocyte sedimentation rate (ESR)

Hemolytic anemia is a condition marked by the accelerated destruction of erythrocytes or red blood cells (RBCs) in the body, resulting in a reduced number of circulating RBCs. Premature destruction of these cells can lead to a range of symptoms and complications, including fatigue, fever, dizziness, jaundice, dark urine, tachycardia, enlarged spleen (splenomegaly), and liver (hepatomegaly). Clinical assessment, coupled with additional laboratory tests, such as complete blood biometry, are essential for determining the cause and severity of hemolytic anemia. Complete Blood Biometry, a standard blood test, furnishes crucial information about the types and numbers of cells in human blood. Hematology analyzers, employing various technologies like impedance, flow cytometry, and laser light scattering, are pivotal in providing detailed information on red blood cells, white blood cells, and platelets [40].

Hemolytic anemia can influence aggregation and the ESR in diverse ways due to alterations in the composition and characteristics of RBCs. However, these changes are not exclusive to hemolytic anemia; various conditions, including infections, inflammatory disorders, and other types of anemia, can also impact these parameters. Erythrocyte aggregation, a common phenomenon, undergoes significant alterations in several pathophysiological conditions, particularly those associated with inflammation. These conditions lead to changes in the size of aggregates and the rate at which they form [17,41].

Normally, RBCs have a negative surface charge that prevents their aggregation, keeping them dispersed in the blood medium. Erythrocyte aggregation occurs due to electrostatic forces that bring together the negatively charged cells, leading to the formation of stacks of RBCs (phenomenon *Rouleaux*) [42,43]. In certain diseases, the plasma proteins become positively charged, considerably neutralizing the negative surface charges of RBCs and reducing their repulsion force (zeta potential). This reduction in repulsion force facilitates erythrocytes aggregation, consequently increasing their sedimentation rate [1,44].

The proteins promoting erythrocyte aggregation (decreasing the zeta potential) are mainly fibrinogen in high concentrations and globulins, while albumin counteracts aggregation (increasing the zeta potential) [45]. Other studies have also indicated that acute-phase proteins, besides fibrinogen and immunoglobulins, can affect erythrocyte aggregation [46]. According to this mechanism, the ESR tends to be higher in anemic blood due to the imbalance between plasma proteins and the low number of RBCs. Additionally, other factors can interfere with ESR, apart from RBCs properties, hematocrit (HCT), and plasma [47]. Technical factors such as ambient temperature, time from sample collection, tube orientation/tilt, and vibration can affect it. Similarly, icterus, hemolysis, or the intake of certain medicines and supplements may interfere with the results [48].

2. Materials and methods

2.1. Blood samples

Whole blood samples were collected from healthy donors (5 male and 5 female) and individuals clinically diagnosed with hemolytic anemia (5 female), following informed consent procedures and in strict adherence to the Declaration of Helsinki and local statutory requirements (No. DI/22/301/03/40).

Venous blood samples were drawn from the antecubital vein and deposited into Vacutainer tubes containing Ethylenediaminetetraacetic acid (EDTA) (BD Vacutainer, Becton, Dickinson, and Company, New Jersey, USA). In addition, all samples underwent complete blood biometry as part of routine procedures, and serological studies were performed on healthy blood samples. The hematological analyzer used was B40603 - DxH 560 *AL Beckman Coulter brand.*

2.2. The PA metrics

The PA metrics derived from the temporal signals included the PA amplitude of the first peak (PA_{FP}), calculated as the difference between the maximum signal value at that peak and the baseline (the horizontal straight line along the y-axis). The arrival time (t_a) of a PA signal represented the point at which acoustic waves generated by light absorption reached the detection system. Erythrocyte sedimentation time (ESt) measured the time elapsed from sample deposition in the quartz cell to

Table 1
General experimental characteristics of published of ESR and/or RBC aggregation studies in blood samples using the PA technique.

Ref.	Laser characteristics			# Blood Samples			Transducer center frequency	Results
	λ (nm)	Pulse Size (ns)/ Repetition Rate (Hz)	Fluence (mJ/ cm^2)	Animals	Human	+ Solutions	[MHz]	
(25,30)	750 and 1064	6 / 10	25	1 (Porcine)	—	Dextran	5	Detection of induced aggregation and oxygenation levels of porcine RBCs.
(20)	1064	6 / 10	25	1 (Porcine)	1	Dextran-PBS	5	Detection of induced aggregation artificially with dextran of human (a single donor) and porcine RBCs, theoretically and experimentally.
(33)	1064	6 / 10	314	—	1 (A single donor from Innovative Research Inc.)	Dextran- PBS	5	Detection and quantification of induced aggregation artificially of RBC in various concentration of Dextran-70. The study was performed just one human blood sample.
(21)	632.8	CW-laser modulated by a chopper at 11 Hz	—	Fish	—	—	—	Study of the dynamics of blood and hemolymph sedimentation in real time using the CW PA technique.
(23,24)	1064	<10 / 500	≈ 106 μJ delivered through ~2 mm, optical fiber	—	1 (male, 33 years)	Dextran-PBS	1	Monitoring of blood sedimentation dynamics *in vitro* experiments using dextran to induce artificially aggregation of RBC from 1 male.
(38)	CW-laser:532 OPO: 415–2300	CW-laser: 12/- OPO: 8/-	CW-laser: 100–7000 OPO: $100–1\times10^5$	White Fisher (F344) rats	Cells of the MDA-MB-231 human breast adenocarcinoma cell line	De-ionized water	3–6	Monitoring of the sedimentation kinetics of individual live cells and single absorbing micro-particles. Cells where from White Fisher (F344) rats and MDA-MB-231 human breast adenocarcinoma cell line
(34)	700 – 900 using the VevoLAZR imaging system.	—	Optical fiber.	—	3	0.9% saline solution	—	Study of the λ-dependence of quantitative PA assessment of the pulsatile blood flow considering the relationship between RBC aggregation and sO_2. The pulsatile blood flow was investigated in vivo on the arm of 3 voluntaries and, the energy laser was delivery thought an optical fiber.
(35)	532	330 ps/4kH	20–150	—	1	The coupling fluid: Dulbecco's modified Eagle's medium (DMEM) - PBS	Pulse-echo ultrasound from 100–1000	Study of the size and morphology of RBCs using high-frequency PA spectral features with a very low sample size.
(39)	CW-Laser: 460. Pulsed Laser: 532	CW-Laser: 5 MHz. Pulsed-Laser: 5 / 10	CW-Laser: <1.6 W, 4 mm^2 Pulsed-Laser: 37.5	—	Healthy donors	Isotonic, hypotonic, and hypertonic	3.5–3.8	Detection the quantitative and the morphological changes in RBCs. Three different salt (NaCl) solutions were added in the blood to induced morphological changes in RBCs. The study compared pulsed and CW laser-based PA signal response technique.
(27,29)	700, 750, 800, 850, and 900 nm	10 / 20	< 5	—	The radial artery of 12 Healthy adults	—	A 256-element linear-array transducer with a central frequency of 21 MHz	Study in vivo of the relation between the sO_2 and hemodynamic behavior such as RBC aggregation during a cardiac cycle in healthy volunteers.
(22, 37)	—	—	—	—	—	—	—	Studies related to the monitoring of sedimentation and/or aggregation using particles or simulations by PA.

when the PA signal reached the baseline. The linear slope (LS) corresponded to the linear interval of the sigmoid curve obtained by plotting normalized PA_{FP} vs ESt. The ESR in our method was determined by measuring the time (ESt) in which RBCs traveled a certain distance (d) inside a quartz cuvette, mathematically expressed as ESR = d / ESt (mm/hr). The initial position marked the upper limit of the homogenized blood sample, and the final position was identified where the PA signal reached baseline, this meant that RBCs had settled, and the laser spot was incident on the plasma.

Additionally, we employed a frequency-domain analysis, a commonly used method to study the spectral content of PA signals. ESR was analyzed using the power spectrum density (PSD) of the measured signal. The PSD was computed in the frequency range from 0 Hz to 4.6 MHz, and a linear model $PS_{lin}(f) = Sf + I$ was fitted from the PSD. The associated slope S in dB/MHz and intercept I measured in dB were obtained. Furthermore, the relative change in the slope S_r and intercept I_r were calculated as the spectral parameters. Finally, considering a time window of T =25 min, the rate of change of the spectral parameters was computed as, $\delta_S = S_r/T$ and $\delta_I = I_r/T$, for the slope and intercept, respectively. These rates of change served as the characteristic features that distinguished healthy and anemic blood samples.

2.3. Experimental setup

The experimental setup is shown in Fig. 1. A Q-Switched Nd:YAG laser (*Brilliant B, Quantel, Bozeman, Montana, USA*) emitting at 532 nm, 5 ns pulse width, and 10 Hz pulse repetition was employed. The energy per pulse was approximately 1.8 mJ (*UM-B, Gentec-EO, Quebec, Canada*) with a spot diameter of 0.4 cm and 14.32 mJ/cm^2 fluence per pulse. A broadband polyvinylidene fluoride (*PVDF*) transducer (*LDT1–028 K, TE Connectivity Company, Mansfield, Texas USA*) with a center frequency of 3.2 MHz was used to detect the ultrasound waves. The PA signals were displayed on a digital oscilloscope with 2 GHz bandwidth (*DPO 5204B, Tektronix, Inc., Beaverton, Oregon, USA*), triggered by a Si photodiode with fixed gain and a wavelength range of 200–1100 nm (*PDA10A, Thorlabs, Inc., New Jersey, USA*).

To acquire PA signals, the whole blood sample within in the Vacutainer tube (approximately 3 ml) was carefully placed in a quartz spectrophotometric cuvette (*Z276669, Sigma-Aldrich, Merck KGaA, Darmstadt, Germany*), whose position was kept fixed by a custom-made plastic container. The quartz cuvette, with a volume of 3.5 ml and L 12.5 x W 12.5 x H 48 mm, featured an optical path length of 10 mm and a spectral transmission range of 170–2700 nm. PA detection followed a forward mode; that means, the sensor was aligned in the same direction as the laser incidence. Thus, on one side of the quartz cell, the light was incident and on the back side, the PVDF piezoelectric transducer was coupled with double-sided tape. The laser spot was consistently directed at the quartz cuvette, located one cm below its midpoint on the vertical axis, and no additional system was required to amplify the PA signal.

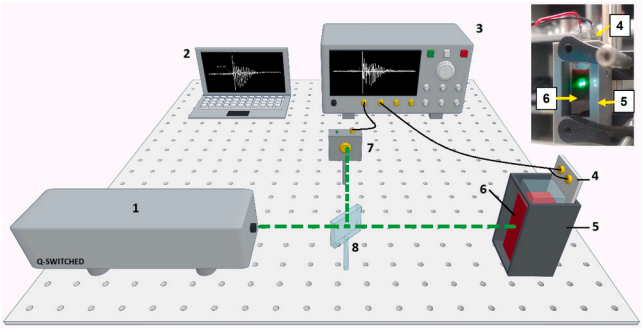

Fig. 1. The experimental PA setup (drawing not to scale). 1. Q-Switched Nd:YAG Laser. 2. Personal computer. 3. Oscilloscope. 4. Polyvinylidene fluoride (PVDF) transducer. 5. Custom-made plastic container for quartz cuvette. 6. Quartz cuvette with a blood sample. 7. Photodiode. 8. Beam splitter. A photograph of the cuvette and transducer arrangement is shown in the inset.

Before each PA measurement, the blood sample was homogenized with the anticoagulant, employing gentle oscillatory movements of the tube to prevent hemolysis. After depositing the sample in the quartz cuvette, PA signals from the blood of healthy females (BHW), healthy males (BHM), and females diagnosed with hemolytic anemia (BAW) were recorded at intervals of 0, 1, 2, 4, or 8 minutes.

2.4. Statistical analysis

The statistical analysis was conducted using the Statistical Package for the Social Science, SPSS version 21 (*Armonk NY: IBM*). Despite the small sample size of our study, the data exhibited a normal distribution, as determined by the Shapiro-Wilk test. Furthermore, the student *t*-test was employed to assess differences between groups (blood with and without pathology) at a 95% confidence level. All results were presented as means ± standard deviation (SD).

3. Results

3.1. PA signals at ESt=0

Following the deposition of the blood sample into the quartz cuvette, recording of the PA signals commenced. Fig. 2 illustrates the average PA signal and its standard deviation (grey shadow) at ESt=0 (initial PA signal recording) for (a) BHW and (b) BHM. The temporal profile of the complete PA signals is shown in the inset of each figure. The PA signals were grouped by sex since it is well known that the levels of hemoglobin (Hb) and RBCs vary with the age and sex of the subject [49]. Fig. 3 displays the PA signals of BAW, accompanied by the inset of Fig. 3, which exhibits the concentration of RBCs per microliter and Hb per g/dl derived from complete blood biometry.

Fig. 4 (left axis) shows the PA amplitude of the first peak (PA_{FP}) as a function of (a) RBCs, (b) Hb concentration, and (c) % HCT for all samples studied. Hematological laboratory values obtained from complete blood biometry reveal a non-linear increase in PA_{FP} with rising hematological variables. Notably, the most significant distinction between healthy blood samples (BHW and BHM) and blood samples with anemia occurs in Hb concentration and % HCT (Fig. 4(b) and 4 (c)). Statistical analysis using the t-student test demonstrates a significant difference in the PA_{FP} ($p < .0001$) between healthy blood and anemic blood.

3.2. Speed of sound (SOS, v_s)

The speed of sound (v_s) for each blood sample was calculated from the arrival time (t_a) of the PA signal. The arrival time is obtained directly from the signal recorded by the oscilloscope, then: $v_s = d_c/(t_a - \Delta t_q)$, where d_c = 10 mm quartz cuvette thickness, Δt_q is the time due to SOS through one of the cell walls [50]. Only the thickness of the cell wall that is in direct contact with the sensor is considered.

Fig. 4 (right axis, red) shows, in turn, the SOS as a function of the concentration of (a) RBCs, (b) Hb, and (c) % HCT for each blood sample. The average SOS for all samples was 1573 ± 5 m/s; aligning with values reported in other studies [51,52]. The *t*-student test indicates a significant difference in SOS between healthy blood (1577 ± 2 m/s) (from women and men), and blood from women with anemia (1567 ± 6 m/s) ($p < 0.05$).

3.3. PA signals during ESt

Distinct ESt values were obtained based on the sample under study. The ESt was the time during which the PA signals were recorded during the sedimentation process, from the time the blood was deposited in the quartz cell (ESt=0) until the PA signal reached the baseline due to the

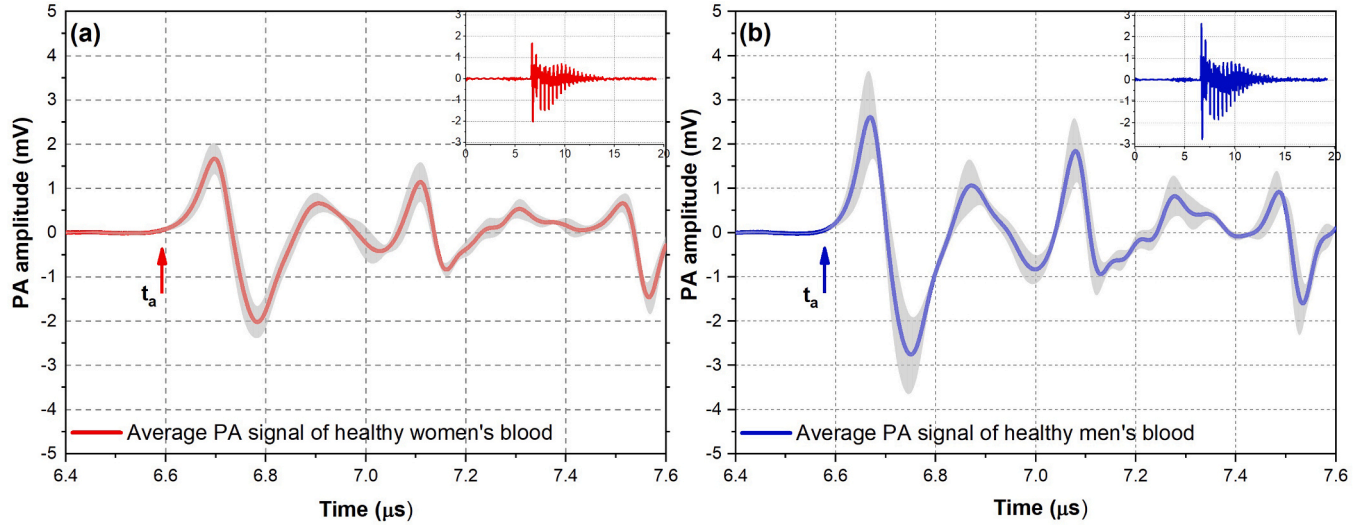

Fig. 2. The average PA signal and standard deviation (shadow) from healthy blood of (a) 5 women and (b) 5 men; t_a= arrival time. The temporal profile of the complete PA signals is shown in the inset of each figure.

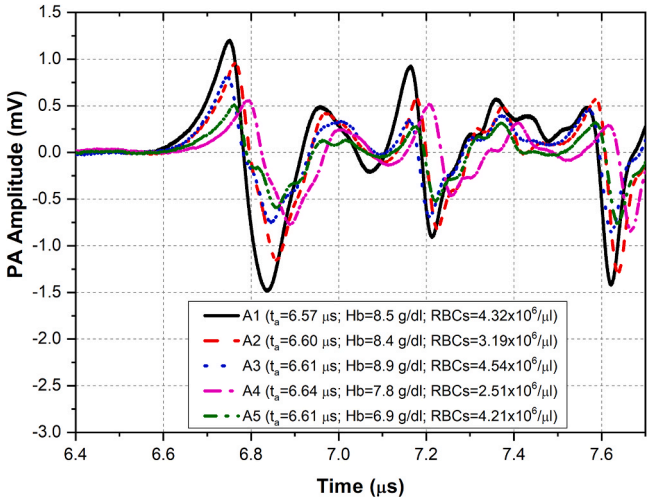

Fig. 3. The PA signals of blood with hemolytic anemia from women. Hemoglobin (Hb), Erythrocytes (RBCs). Ai= 1,…,5 corresponds to each sample.

laser practically hitting the plasma (Fig. 5(a)). Fig. 5 illustrates the PA signals during erythrocyte sedimentation for healthy whole blood samples from (b) a woman (ESt=56 min), (c) a man (ESt=148 min), and (d) a woman with hemolytic anemia (ESt=42 min). In this case, the ESt for the healthy whole blood samples was approximately 2.5 times higher for the male than the female, and 3.5 times higher than for the blood of the female with anemia. Higher ESt values correspond to lower ESR, consistent with findings in anemia and acute-phase protein-related disease [48,53].

Fig. 6 displays the average normalized PA_{FP} amplitude with standard deviation for BHW, BHM, and BAW as a function of ESt, along with their respective sigmoid-shaped fit curves [54]. The ESR mean values were (4.74 ± 3.29) mm/h for BHM, (10.9 ± 4.89) mm/h for BHW, and (17.06 ± 5.25) mm/h for BAW. Despite high SD, a significant difference was obtained between healthy blood (from men and women) and anemic blood from women ($p < 0.05$) according to the t-student test.

Linear regression analysis was performed in each mean curve of Fig. 6, corresponding to the sedimentation phase (linear region of the curve). The linear regression analysis for BHM was conducted within the time range of [24−96] minutes, for BWH within [12−44] minutes, and for BAW within [6−28] minutes. The selection of these specific time

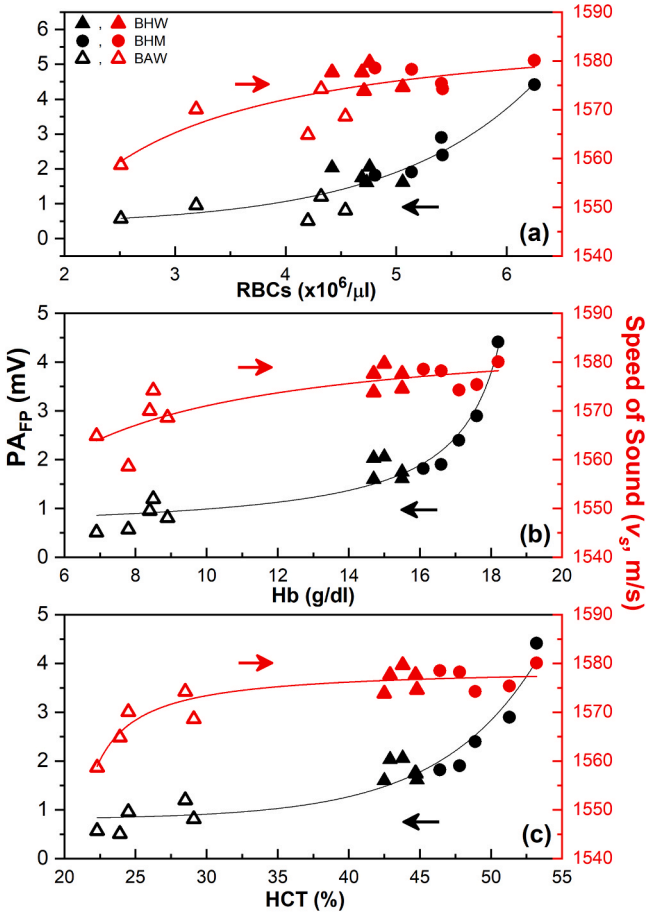

Fig. 4. The PA_{FP} (left axis, black) and SOS (right axis, red) as a function of the concentration of (a) RBCs, (b) Hb, and (c) % HCT, for each sample.

intervals was determined by aligning with the observed precipitation phases in each group. The values of linear slopes (LS) were −0.024 ± 0.007 (r=−0.998), −0.012 ± 0.006 (r=−0.996), and −0.033 ± 0.009 (r=−0.994) a.u/min for BHW, BHM, and BAW, respectively. A significant difference in LS was obtained between healthy blood (from men and women) and anemic blood from women ($p < 0.05$) according to the

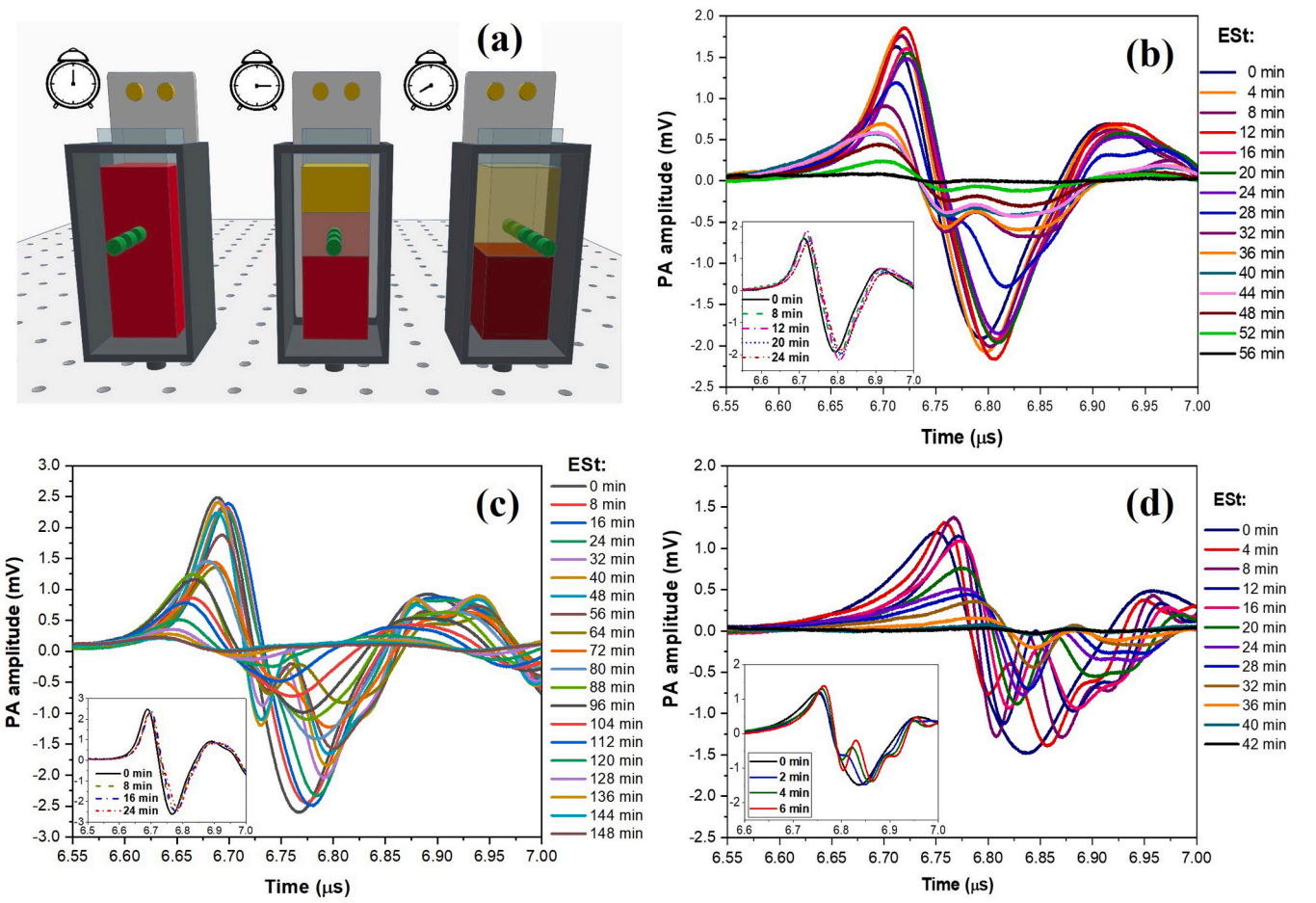

Fig. 5. (a) Illustrative image of the quartz cuvette coupled with the PVDF transducer inside a container during 3 different times: at the beginning (ESt=0, left), during (middle), and end (right) of blood sedimentation; the laser incidence was forward and remained fixed. PA signals during the erythrocyte sedimentation process of healthy blood from (b) a woman, (c) a man, and (d) a woman with hemolytic anemia. The lower boxes of the figures show their respective signals during the first 24 minutes for healthy blood (female and male) and the first 6 minutes for blood with anemia.

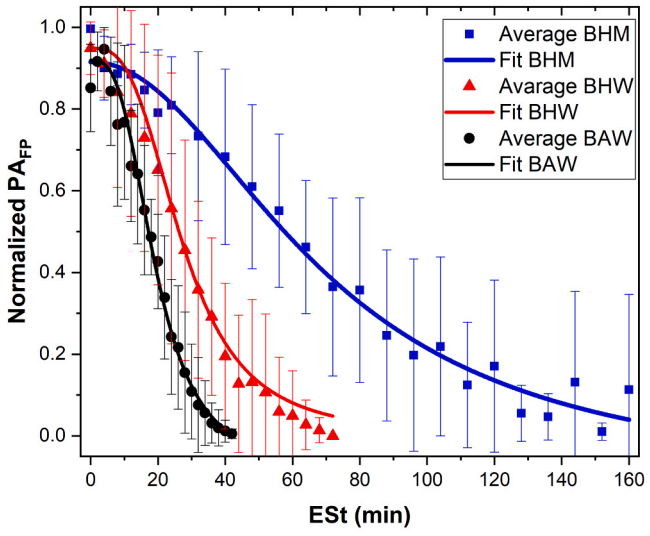

Fig. 6. Normalized PA_{FP} with its standard deviation of BHW (triangle), BHM (square), and BAW (circle) as a function of ESt.

t-student test.

Table 2 summarizes the mean and standard deviation of participant age, RBCs, Hb, and % HTC, and all the variables obtained from the PA signals of the BHW, BHM, and BAW samples. The t-test results indicate that there is a statistically significant difference between healthy blood and hemolytic anemic blood in all hematological and temporal PA parameters except ESt.

3.4. Spectral analysis of PA signals for monitoring ESR

To quantitatively assess the dynamic changes in the PA signals during the initial minutes, a spectral analysis was conducted using a methodology previously employed in the study of biological tissues [55–57]. Specifically, the power spectrum density (PSD) within a time-domain window of 6.55–7 μs from the PA signals was calculated. Subsequently, a linear model with the form $PS_{lin}(f) = Sf + I$ derived from the PSD within a 4.6 MHz bandwidth, where S represents the slope in dB/MHz, and intercept I represent the intercept in dB, within the frequency range f. These spectral parameters of the model PS_{lin}, allow a characterization of the PA signal [25,58,59].

Fig. 7 shows the PSD of PA signals from BHW (a)-(c), BHM (d)-(f), and BAW (g)-(i) samples. Therein, we only show the spectra of relevant time instants during monitoring for a single experiment, for illustrative purposes. Notably, the PSD of healthy samples (BHW and BHM) exhibits negligible change. In contrast, the PSD of BAW samples decreases over time, indicating a reduction in PA signal amplitude in the time domain (see Fig. 5). Specifically, a rapid decrease in magnitude is observed in anemic blood (BAW) compared to healthy blood at 8 minutes and 25 minutes of monitoring. While this observation provides valuable

Table 2
The mean and SD of the age of the participants, the values of RBCs, Hb, %HTC, and temporal and spectral parameters from PA signals of BHW, BHM, and BAW samples.

Parameters	Healthy women's blood (BHW) (N = 5) M ± SD	Healthy men's Blood (BHM) (N = 5) M ± SD	Blood from anemic women (BAW) (N = 5) M ± SD	P
Age (years)	31 ± 8	31 ± 7	34 ± 9	
RBCs (x10^6/μL) Reference Interval [4.5–5.2]	4.7 ± 0.2	5.4 ± 0.5	3.7 ± 0.8	
RBCs (healthy/ anemia)	5.1 ± 0.5		3.7 ± 0.8	.023
Hb (g/dL) Reference Interval [11–18.8]	15.0 ± 0.4	17.1 ± 0.8	8.1 ± 0.8	
Hb (healthy/ anemia)	16.1 ± 1.2		8.1 ± 0.8	<.0001
HTC (%) Reference Interval [35–55.5]	43.7 ± 1.0	49.5 ± 2.7	25.7± 3	
HCT (healthy/ anemia)	46.6 ± 3.6		25.7± 3	<.0001
PA_{FP} (mV)	1.8 ± 0.2	2.7 ± 1.0	0.8 ± 0.3	
PA_{FP} (healthy/ anemia)	2.2 ± 0.8		0.8 ± 0.3	<.0001
t_a (μs)	6.57 ± 0.01	6.56 ± 0.01	6.60 ± 0.02	
t_a (healthy/ anemia)	6.57 ± 0.01		6.60 ± 0.02	<.0001
ESt (min)	50.0 ± 17.8	135.6 ± 80.7	31.8 ± 7.4	
ESt (healthy/ anemia)	92.8 ± 71.2		31.8 ± 7.4	.084
LS (min^{-1})	-0.024 ± 0.007	-0.012 ± 0.006	-0.033 ± 0.009	
LS (healthy/ anemia)	-0.019 ± 009		-0.033 ± 0.009	0.020
v_s (m/s)	1576 ± 2	1577 ± 2	1567 ± 6	
v_s (healthy/ anemia)	1577 ± 2		1567 ± 6	<.0001
ESR (mm/hr)	10.90 ± 4.89	4.74 ± 3.29	17.06 ± 5.25	
ESR (healthy/ anemia)	7.82 ± 5.10		17.06 ± 5.25	.012
δ_S (%/min)	0.0489 ± 0.0672	0.0333 ± 0.0553	1.0035 ± 0.1540	
δ_I (%/min)	0.0462 ± 0.0358	0.0365 ± 0.0402	0.3683 ± 0.1344	

Note: PA_{FP}= PA amplitude of the first peak; v_s= speed of sound; t_a= arrival time; LS= linear slope; ESt= Erythrocyte sedimentation time; ESR= Erythrocyte sedimentation rate; δ_S =Change in spectral slope; δ_I = Change in spectral intercept.

insights, which could be related to the effective absorber, it is limited in providing a quantitative analysis. Therefore, the spectral parameters of the linear model (straight lines in Fig. 7) offer a simple yet effective approach to quantifying changes in PA signals.

Our hypothesis posits that a simple linear model can distinguish between healthy and anemic blood samples based on the PSD of PA signals. The decrease in PA signal magnitude over time suggests a potential utility of spectral parameters for faster quantification compared to traditional methods to calculate ESR. Specifically, only two parameters, the S_r and intercept I_r would be necessary to track those changes. Thus, the relative difference for the slope S_r and intercept I_r was calculated as follows,

$$S_r = \left|1 - \frac{S_x}{S_o}\right| \cdot 100\%,$$

$$I_r = \left|1 - \frac{I_x}{I_o}\right| \cdot 100\%,$$

where, the subscript x refers to the measurement at a time $t > 0$, and the quantities S_o and I_o are the parameters retrieved at $t = 0$, which serve as the reference data. The above relationships allow us to measure the rate of change in the PSD magnitude, which encodes the structural features of the blood sample under study.

Fig. 8 presents the behavior of the spectral parameters as a function of monitoring time for BHW, BHM, and BAW over a 25-minute window. Fig. 8 (a) shows the rate of change in the spectral slope, whereas Fig. 8 (b) shows the change in the spectral intercept of the three groups. Notably, both the slope and intercept serve as effective parameters to quantify the change in PA signals from the beginning to the end of the experiment. Hence, it is evident that a substantial change in the PA signal could differentiate healthy samples from hemolytic anemia within a relatively short time interval. Furthermore, from Fig. 8 it is possible to see an almost constant behavior of the spectral parameters for samples BHW and BHM, given by the mean value denoted by the dashed line. Whereas the spectral parameters for BAW exhibit a growing behavior since the start of monitoring, showing an increment of around 6%.

This situation could confirm the hypothesis given that in blood without any pathology, the RBCs are evenly distributed, forming chains that increase in length when they fall to the container's bottom. Whereas, in blood with anemia, RBCs clump together more rapidly, forming aggregates in the first minutes. Hence, both situations are captured by the PA signal, and monitored by the proposed spectral parameters during the globular sedimentation time. To provide quantitative results, we calculated for all the patients, the rate of change in a time window T as, $\delta_S = S_r/T$ and $\delta_I = I_r/T$, for the slope and intercept, respectively.

To confirm that the PA signals are a useful tool for monitoring the ESR, the rate of change in spectral parameters δ_S and δ_I over 25 minutes was analyzed using a one-factor ANOVA with a significance level of $p < 0.05$. Fig. 9 shows scatter plots for the change in spectral slope (a) and intercept (b), for the three groups (BHW, BHM, and BAW). Each dot represents the value of a sample, and the horizontal bar indicates the mean value. Statistical analysis, denoted by *** ($p < 0.001$), confirms that the change in spectral parameters effectively differentiates between healthy and diseased samples within a short 25-minute monitoring period, requiring less time than the classical ESR measurement methods.

To validate the cellular integrity of red blood cells (RBCs) before and after laser incidence, a smear was prepared using the trypan blue staining method [60]. Cell viability was confirmed through optical microscope examination. Fig. 10 displays images of the smear for a healthy blood sample (a) and one with anemia (b) before (top pictures) and after (bottom pictures) sedimentation. The blood drop from the smear after sedimentation was obtained from the bottom of the quartz cuvette.

As can be seen, in Fig. 10 (a), RBCs of healthy blood are uniformly distributed on the slide while in the blood with anemia, Fig. 10 (b), the Rouleaux phenomenon is intensified. The formation of large clusters of RBCs with different morphologies could be associated with pathologies affecting microcirculation. This comprehensive analysis reinforces the utility of PA signals and spectral parameters for discerning subtle variations in blood composition and structural characteristics.

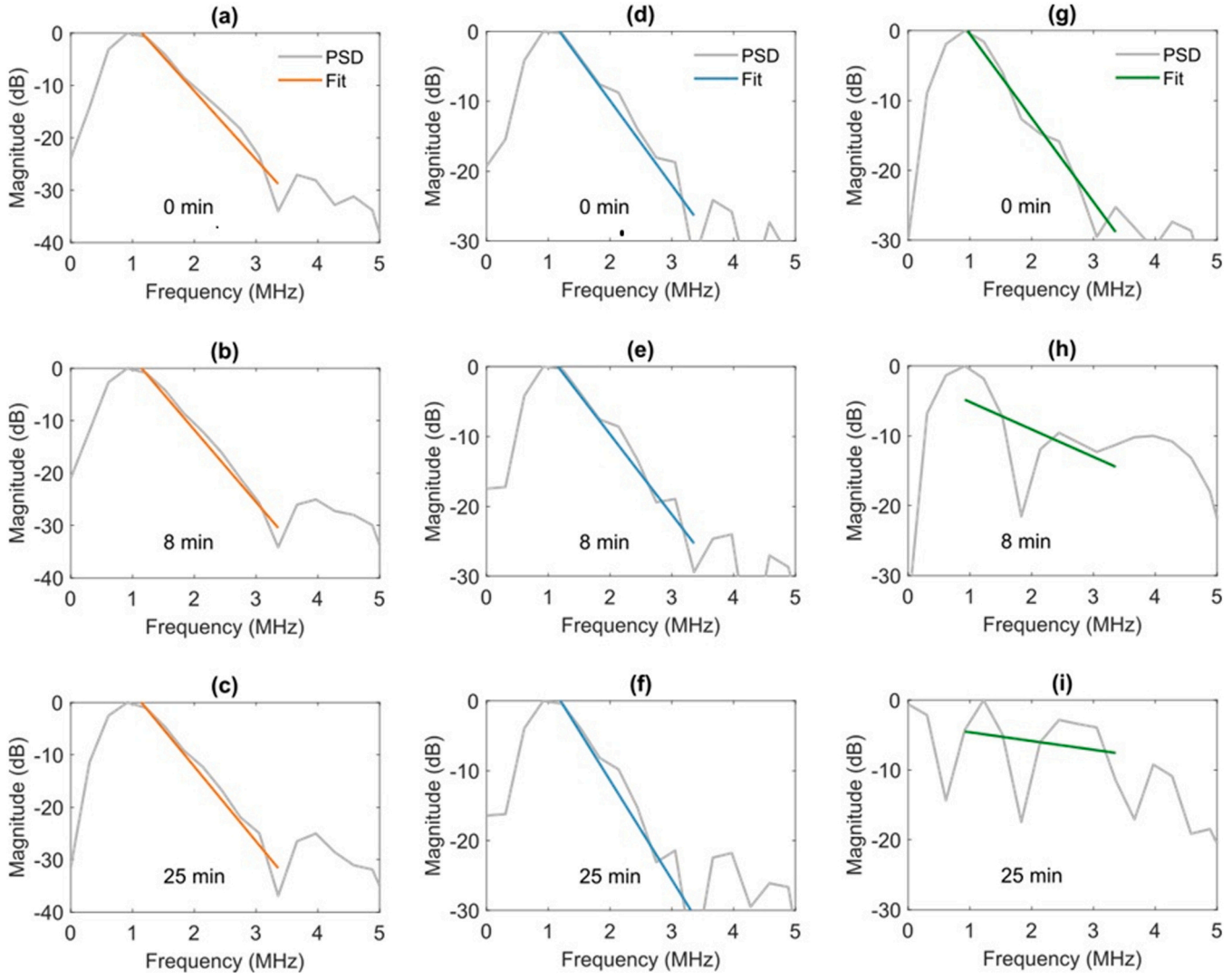

Fig. 7. Power spectrum density and the fitted linear model for (a)-(c) BHW, (d)-(f) BHM, and (g)-(i) BAW, in three relevant time instants for monitoring the PA signal.

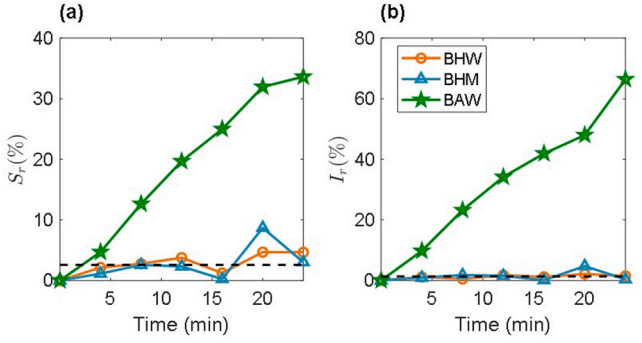

Fig. 8. Rate of change in the spectral parameters, (a) slope S_r and (b) intercept I_r as a function of monitoring time for BHW, BHM, and BAW.

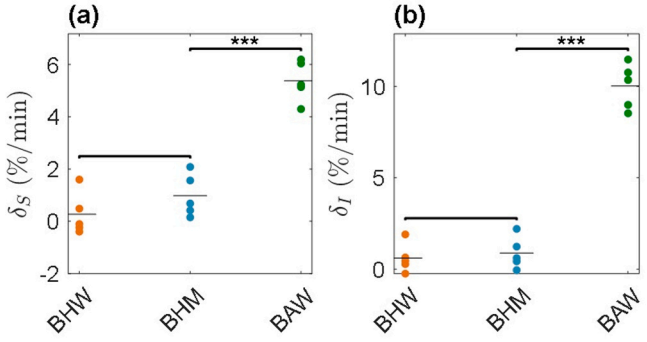

Fig. 9. Scatter plot of the statistical analysis in the change of spectral parameters: (a) slope δ_S and intercept δ_I.The statistical significance is explained by *** $p < 0.001$ to differentiate among whole blood groups.

4. Discussion

4.1. PA signals at ESt=0

Fig. 2 show that the temporal profiles of the average PA signals for both healthy (a) women's and (b) men's blood samples exhibit remarkable similarity, despite inherent biological variability within each sample. Notably, the primary distinctions between these PA signals or PA signatures are found in the amplitude and the arrival time (t_a). The amplitude of the PA signal is influenced by factors such as the tissue's optical absorption coefficient, fluence, and a temperature-dependent

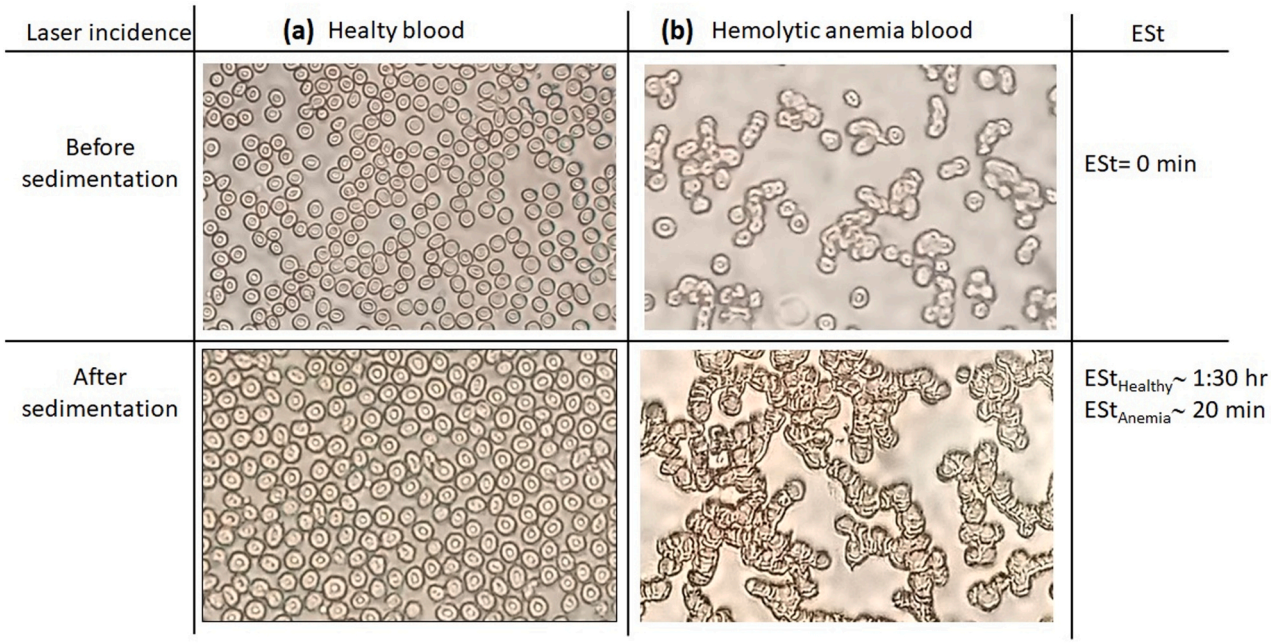

Fig. 10. Pictures of RBCs before (up) and after (down) the sedimentation process (x40) from a) a healthy blood and, b) a hemolytic anemia blood.

coefficient known as the Grüneisen parameter [61]. Given these last two parameters are constant, it can be deduced that the pivotal factors influencing variations in PA amplitude are the hemoglobin (Hb), hematocrit (HCT), and red blood cells (RBCs), namely, where the absorbing chromophore is [24]. On the other hand, it is well-established that Hb levels in women are approximately 12% lower than in men mainly due to hormonal factors [62]. Consequently, this gender-based discrepancy results in a higher amplitude of the PA_{FP} signal in men than in women.

In the PA signals of BAW (Fig. 3), discerning a clear pattern or PA signature akin to healthy blood samples becomes challenging. It can be noted that the amplitudes of these signals are lower than those observed in healthy blood samples, particularly when comparing them with the average PA signal of BHW, whose mean PA_{FP} value is approximately 1.8 mV. In contrast, the mean PA_{FP} value BAW is notably reduced, at around 0.8 mV.

The diminished amplitudes in BAW samples can be attributed to lower Hb levels and % HCT due to reduced red blood cell production, leading to decreased blood density (Fig. 4, left axis). Additionally, the arrival time (t_a) of the PA signal varies slightly in each case, in contrast to the consistent pattern observed in healthy blood samples, where the variation is approximately 10 ns. For anemic samples, this variation increases to 20 ns, indicating a lower SOS and further underscoring the distinctive characteristics of blood samples affected by anemia.

4.2. Speed of sound (SOS)

In Fig. 4, SOS (right axis) is observed to increase as a function of (a) RBCs, (b) Hb, and (c) % HCT. However, the relationship does not appear to be strictly linear. This non-linear behavior may be attributed to the density of RBCs in the sample, where a higher cell count implies a smaller mean free path between cells, leading to an increase in the propagation velocity of the acoustic wave. This explains the higher SOS value (v_s) observed in samples from healthy individuals compared to those with anemia. Bradley et al. found a linear relationship between ultrasonic transmission velocity and hematocrit, temperature, and total protein [52].

4.3. PA signals during ESt

Despite varying average ESt durations ranging from 31.8 minutes (anemia) to 135.6 minutes (men without pathology), the PA signal analysis provides additional insights not captured by conventional techniques. Fig. 5(b), (c), and (d) reveal distinct characteristics during the sedimentation process of 3 samples. In healthy blood, both male and female, the PA signal remains practically stable for the initial 24 minutes (the inset of Fig. 5(b) and (c)), after which changes in amplitude and shape occur, presenting a slight ripple in the first minimum of both signals. Conversely, blood from a woman with hemolytic anemia (the inset of Fig. 5(d)) shows changes in the PA signal from the first minute, with a noticeable ripple in the first minimum. This behavior was similar in all samples of each group.

Furthermore, a subtle temporal shift of signal peaks during sedimentation is observed to the right for anemic blood and the left for healthy blood. This temporal shift is attributed to multiple factors, such as, variations in particle concentration, alterations in particle size and shape, changes in particle-related optical properties, interactions among particles, and temperature and pressure conditions. Maintaining constant temperature and pressure, the primary factors contributing to the temporal shift are believed to be interactions among erythrocytes and their distribution. Notably, erythrocyte orientation and morphology, as reported by Strohm et al. [35,63] can impact the photoacoustic signal, suggesting potential diagnostic implications for red cell-related diseases and infections.

The distribution of RBCs during erythrocyte sedimentation varies between healthy blood and blood with anemia. In healthy blood, RBCs form isolated cells or chains that increase in length as they settle, while RBCs in blood with anemia clump together more rapidly, forming aggregates within the first few minutes [64]. This behavior, observed in both experimental studies and theoretical simulations [20], underscores the potential of measuring pressure waves generated by light absorption to assess the spatial organization of cells and the level of aggregation [21].

Erythrocyte sedimentation in blood with anemia involves processes affecting the cell membrane's integrity and intracellular boundaries of RBCs. Hemolysis rates are higher in hemolytic anemia, resulting in irregularly shaped RBC conglomerates that are prematurely destroyed

[65]. The aggregation ability, influenced by hematocrit, RBCs, and plasma factors, leads to a faster sedimentation rate in hemolytic blood than in healthy blood. However, the factors determining erythrocyte sedimentation rate (ESR) remain unclear, with evidence suggesting that abnormalities in RBC shape, size, and rigidity can inhibit the formation of Rouleaux and irregular aggregates, resulting in a slower sedimentation rate, as seen in sickle cell anemia [66–69].

Finally, the results derived from the spectral parameters underscore the potential of photoacoustic signal proposed analysis as a rapid and dependable tool for evaluating human blood samples in clinical contexts, paving the way for more precise and sensitive diagnostic methodologies. While conventional tests for calculating ESR often fall short in enabling specific diagnoses, the adaptability of the PA technique has facilitated the exploration of signal analysis methods that offer classification parameters, providing valuable insights into diverse physiological conditions within the bloodstream [70].

5. Conclusions

In this study, we innovatively developed a photoacoustic (PA)–based methodology for analyzing blood samples from individuals without clinical pathology and those diagnosed with hemolytic anemia. Our approach was based on analyzing both temporal and spectral parameters of raw photoacoustic signals, taking advantage of a customized experimental setup. Remarkably, this method eliminates the need for prior blood preparation. Our results reveal significant statistical differences in temporal and spectral PA parameters between healthy and anemic blood samples.

The study of erythrocyte sedimentation rate (ESR) through the analysis of PA signals emerges as an appealing tool, delivering conclusive results in a remarkably shorter timeframe than traditional techniques, which yield only an ESR value after an hour. This contribution holds promise for developing precise and sensitive methods in clinical settings for scrutinizing human blood samples. Additionally, our preliminary study allowed us to assess the feasibility and challenges of the technique for blood analysis. Enhancements in sample size and blood quantity, standardizing the process, are anticipated to refine and augment the preliminary findings of our work.

CRediT authorship contribution statement

Argelia Pérez-Pacheco: Conceptualization, Formal analysis, Investigation, Methodology, Project administration, Validation, Visualization, Writing – original draft, Writing – review & editing. **Roberto G. Ramírez-Chavarría:** Formal analysis, Funding acquisition, Investigation, Methodology, Writing – original draft, Writing – review & editing. **Marco Polo Colín-García:** Methodology, Visualization, Writing – original draft. **Flor del Carmen Cortés-Ortegón:** Methodology, Validation, Visualization, Writing – original draft. **Rosa María Quispe-Siccha:** Conceptualization, Investigation, Visualization, Writing – original draft, Writing – review & editing. **Adolfo Martínez-Tovar:** Conceptualization, Methodology, Supervision, Validation, Visualization, Writing – original draft. **Irma Olarte-Carrillo:** Investigation, Methodology, Supervision, Validation, Writing – original draft. **Luis Polo-Parada:** Supervision, Validation, Visualization, Writing – original draft, Writing – review & editing. **Gerardo Gutiérrez-Juárez:** Investigation, Supervision, Validation, Visualization, Writing – original draft, Writing – review & editing.

Declaration of Competing Interest

The authors declare that they have no known competing financial interests or personal relationships that could have appeared to influence the work reported in this paper.

Data availability

Data will be made available on request.

Acknowledgments

This study was supported by the grants UNAM -PAPIIT TA101423, 1N101821, and project Fronteras de la Ciencia 2016–2 No. 2029 CONACyT. We express our thanks to the Blood Bank at Hospital General de México “Dr. Eduardo Liceaga” for their valuable help in carrying out this work.

Statement

The data is available to access.

References

[1] R.Ben Ami, G. Barshtein, D. Zeltser, Y. Goldberg, I. Shapira, A. Roth, et al., Parameters of red blood cell aggregation as correlates of the inflammatory state, Am. J. Physiol. - Hear Circ. Physiol. 280 (2001) 1982–1988, https://doi.org/10.1152/ajpheart.2001.280.5.h1982.
[2] A. Grzybowski, J. Sak, A short history of the discovery of the erythrocyte sedimentation rate, Int J. Lab Hematol. 34 (2012) 442–444, https://doi.org/10.1111/j.1751-553X.2012.01430.x.
[3] G. Eriksen, Erythrocyte sedimentation rate: a possible marker of atherosclerosis and a strong predictor of coronary heart disease mortality, Eur. Heart J. 21 (2000) 1614–1620, https://doi.org/10.1053/euhj.2000.2148.
[4] C. Pathol, ICSH recommendations for measurement of erythrocyte sedimentation rate. J. Clin. Pathol. 46 (1993) 198–203.
[5] M.L. Brigden, Clinical utility of the erythrocyte sedimentation rate, Am. Fam. Physician 60 (1999) 1443–1450.
[6] B.S. Bull, M. Caswell, E. Ernst, J.M. Jou, A. Kallner, J.A. Koepke, et al., ICSH recommendations for measurement of erythrocyte sedimentation rate. J. Clin. Pathol. 46 (1993) 198–203, https://doi.org/10.1136/jcp.46.3.198.
[7] J.M. Jou, S.M. Lewis, C. Briggs, S.H. Lee, B. De La Salle, S. Mcfadden, ICSH review of the measurement of the erythocyte sedimentation rate, Int J. Lab Hematol. 33 (2011) 125–132, https://doi.org/10.1111/j.1751-553X.2011.01302.x.
[8] P. Foresto, M. D'Arrigo, L. Carreras, R.E. Cuezzo, J. Valverde, R. Rasia, Evaluation of red blood cell aggregation in diabetes by computerized image analysis, Med. (B Aires) 60 (2000) 570–572.
[9] S. CHEN, B. GAVISH, S. ZHANG, Y. MAHLER, S. YEDGAR, Monitoring of erythrocyte aggregate morphology under flow by computerized image analysis, Biorheology 32 (1995) 487–496, https://doi.org/10.1016/0006-355X(95)00025-5.
[10] L.E. Böttiger, C.A. Svedberg, Normal Erythrocyte Sedimentation Rate and Age, Br. Med J. 2 (1967) 85–87, https://doi.org/10.1136/bmj.2.5544.85.
[11] S.P. Batlivala, Focus on Diagnosis: The Erythrocyte Sedimentation Rate and the C-reactive Protein Test, Pedia Rev. 30 (2009) 72–74, https://doi.org/10.1542/pir.30-2-72.
[12] C. Wagner, P. Steffen, S. Svetina, Aggregation of red blood cells: From rouleaux to clot formation, Comptes Rendus Phys. 14 (2013) 459–469, https://doi.org/10.1016/j.crhy.2013.04.004.
[13] B. Vennapusa, L.D. Cruz, La, H. Shah, M.L.T. Ascp, V. Michalski, Q.-Y. Zhang, Erythrocyte Sedimentation Rate (ESR) Measured by the Streck ESR-Auto Plus Is Higher Than With the Sediplast Westergren Method A Validation Study, Am. J. Clin. Pathol. 135 (2011) 386–390, https://doi.org/10.1309/AJCP48YXBDGTGXEV.
[14] M.R. Hardeman, P.T. Goedhart, J.G.G. Dobbe, K.P. Lettinga, Laser-assisted optical rotational cell analyser (L.O.R.C.A.); I. A new instrument for measurement of various structural hemorheological parameters, Clin. Hemorheol. Micro 14 (1994) 605–618, https://doi.org/10.3233/CH-1994-14416.
[15] G. Reggiori, G. Occhipinti, A. De Gasperi, J.L. Vincent, M. Piagnerelli, Early alterations of red blood cell rheology in critically ill patients, Crit. Care Med 37 (2009) 3041–3046, https://doi.org/10.1097/CCM.0b013e3181b02b3f.
[16] I. Lapic, E. Piva, F. Spolaore, F. Tosato, M. Pelloso, M. Plebani, Automated measurement of the erythrocyte sedimentation rate: Method validation and comparison, Clin. Chem. Lab Med 57 (2019) 1364–1373, https://doi.org/10.1515/cclm-2019-0204.
[17] O.K. Baskurt, M. Uyuklu, P. Ulker, M. Cengiz, N. Nemeth, T. Alexy, et al., Comparison of three instruments for measuring red blood cell aggregation, Clin. Hemorheol. Micro 43 (2009) 283–298, https://doi.org/10.3233/CH-2009-1240.
[18] P. Gyawali, D. Ziegler, J.F. Cailhier, A. Denault, G. Cloutier, Quantitative Measurement of Erythrocyte Aggregation as a Systemic Inflammatory Marker by Ultrasound Imaging: A Systematic Review, Ultrasound Med Biol. 44 (2018) 1303–1317, https://doi.org/10.1016/j.ultrasmedbio.2018.02.020.
[19] R. Manwar, K. Kratkiewicz, K. Avanaki, Overview of ultrasound detection technologies for photoacoustic imaging, Micromachines 11 (2020) 1–24, https://doi.org/10.3390/mi11070692.

[20] E. Hysi, R.K. Saha, M.C. Kolios, On the use of photoacoustics to detect red blood cell aggregation, Biomed. Opt. Express 3 (2012) 2326, https://doi.org/10.1364/boe.3.002326.
[21] A. Landa, J.J. Alvarado-Gil, G. Gutíerrez-Juárez, M. Vargas-Luna, Photoacoustic monitoring of real time blood and hemolymph sedimentation, Rev. Sci. Instrum. 74 (2003) 377–379, https://doi.org/10.1063/1.1512982.
[22] R.K. Saha, M.C. Kolios, A simulation study on photoacoustic signals from red blood cells, J. Acoust. Soc. Am. 129 (2011) 2935–2943, https://doi.org/10.1121/1.3570946.
[23] Kinnunen M. Monitoring the effect of dextran on blood sedimentation using a pulsed photoacoustic technique. Proc. SPIE, Dyn. Fluctuations Biomed. Photonics IX, vol. 8222, 2012. https://doi.org/10.1117/12.914761.
[24] M. Kinnunen, A pulsed photoacoustic technique for studying red blood cell sedimentation, J. Biomed. Photonics Eng. 1 (2015) 81–89, https://doi.org/10.18287/jbpe-2015-1-1-81.
[25] E. Hysi, R.K. Saha, M.C. Kolios, Photoacoustic ultrasound spectroscopy for assessing red blood cell aggregation and oxygenation, J. Biomed. Opt. 17 (2012) 125006, https://doi.org/10.1117/1.JBO.17.12.125006.
[26] D.A. Kravchuk, K.A. Voronina, Studies of red blood cell aggregation and blood oxygenation on the basis of the optoacoustic effect in biological media, J. Biomed. Photonics Eng. 6 (1) (2020) 5, https://doi.org/10.18287/JBPE20.06.010307.
[27] T.H. Bok, E. Hysi, M. Kolios, Preliminary photoacoustic imaging of the human radial artery for simultaneous assessment of red blood cell aggregation and oxygen saturation in vivo, IEEE Int Ultrason Symp. IUS (2017) 0–3, https://doi.org/10.1109/ULTSYM.2017.8091879.
[28] Y. Zhou, J. Yao, L.V. Wang, Tutorial on photoacoustic tomography, J. Biomed. Opt. 21 (2016) 061007, https://doi.org/10.1117/1.jbo.21.6.061007.
[29] T. Bok, E. Hysi, M.C. Kolios, In vivo photoacoustic assessment of the oxygen saturation changes in the human radial artery: a preliminary study associated with age, J. Biomed. Opt. 26 (2021) 1–14, https://doi.org/10.1117/1.jbo.26.3.036006.
[30] E. Hysi, R.K. Saha, M.C. Kolios, Simultaneous photoacoustic detection of red blood cell aggregation and oxygenation, IEEE Int Ultrason Symp. IUS (2012) 1398–1401, https://doi.org/10.1109/ULTSYM.2012.0349.
[31] E. Hysi, R.K. Saha, M.C. Kolios, On the potential of using photoacoustic spectroscopy to monitor red blood cell aggregation, Dyn. Fluct. Biomed. Photonics IX 8222 (2012) 82220Q, https://doi.org/10.1117/12.928257.
[32] E.I. Galanzha, V.P. Zharov, In vivo photoacoustic and photothermal cytometry for monitoring multiple blood rheology parameters, Cytom. Part A 79 (A) (2011) 746–757, https://doi.org/10.1002/cyto.a.21133.
[33] E. Hysi, R.K. Saha, M.C. Kolios, Characterization of red blood cell aggregation with photoacoustics: A theoretical and experimental study, IEEE Int Ultrason Symp. IUS (2011) 1187–1190, https://doi.org/10.1109/ULTSYM.2011.0292.
[34] T.H. Bok, E. Hysi, M.C. Kolios, In vitro photoacoustic spectroscopy of pulsatile blood flow: Probing the interrelationship between red blood cell aggregation and oxygen saturation, J. Biophotonics 11 (2018), https://doi.org/10.1002/jbio.201700300.
[35] E.M. Strohm, E.S.L. Berndl, M.C. Kolios, Probing red blood cell morphology using high-frequency photoacoustics, Biophys. J. 105 (2013) 59–67, https://doi.org/10.1016/j.bpj.2013.05.037.
[36] C.L. Bayer, S.Y. Nam, Y.-S. Chen, S.Y. Emelianov, Photoacoustic signal amplification through plasmonic nanoparticle aggregation, J. Biomed. Opt. 18 (2013) 016001, https://doi.org/10.1117/1.jbo.18.1.016001.
[37] N.W. Pech-May, J.J. Alvarado-Gil, Photoacoustic monitoring of sedimentation of micro-particles in low viscosity fluids, Rev. Sci. Instrum. 84 (2013), https://doi.org/10.1063/1.4817308.
[38] Kudryashov S.I., Allen S.D., Galanzha E.I., Galitovskaya E., Zharov V.P. Photoacoustics of individual live cells and particles. Photons Plus Ultrasound Imaging Sens 2006 Seventh Conf Biomed Thermoacoustics, Optoacoustics, Acousto-Optics 2006;6086:60860J. https://doi.org/10.1117/12.648559.
[39] A. Gorey, D. Biswas, A. Kumari, S. Gupta, N. Sharma, G.C.K. Chen, et al., Application of continuous-wave photoacoustic sensing to red blood cell morphology, Lasers Med Sci. 34 (2019) 487–494, https://doi.org/10.1007/s10103-018-2621-7.
[40] D.B. DeNicola, Advances in Hematology Analyzers, Top. Companion Anim. Med 26 (2011) 52–61, https://doi.org/10.1053/j.tcam.2011.02.001.
[41] D. Lazari, J.K. Freitas Leal, R. Brock, G. Bosman, The relationship between aggregation and deformability of red blood cells in health and disease, Front Physiol. 11 (2020) 1–6, https://doi.org/10.3389/fphys.2020.00288.
[42] R. Fåhraeus, THE SUSPENSION STABILITY OF THE BLOOD, Physiol. Rev. 9 (1929) 241–274, https://doi.org/10.1152/physrev.1929.9.2.241.
[43] S. Chien, L.A. Sung, Physicochemical basis and clinical implications of red cell aggregation, Clin. Hemorheol. Micro 7 (2016) 71–91, https://doi.org/10.3233/CH-1987-7108.
[44] S. Chien, Electrochemical interactions between erythrocyte surfaces, Thromb. Res 8 (1976) 189–202, https://doi.org/10.1016/0049-3848(76)90062-1.
[45] C.M. Gordon, J.R. Wardley, The effect of the plasma proteins upon the sedimentation rate of human blood, Biochem J. 37 (1943) 393–397, https://doi.org/10.1042/bj0370393.
[46] X. Weng, G. Cloutier, R. Beaulieu, G.O. Roederer, Influence of acute-phase proteins on erythrocyte aggregation, Am. J. Physiol. - Hear Circ. Physiol. 271 (1996), https://doi.org/10.1152/ajpheart.1996.271.6.h2346.
[47] C. Lawrence, M.E. Fabry, Erythrocyte sedimentation rate during steady state and painful crisis in sickle cell anemia, Am. J. Med 81 (1986) 801–808, https://doi.org/10.1016/0002-9343(86)90349-9.
[48] Tishkowski K., Gupta V. Erythrocyte Sedimentation Rate. 2022.
[49] P. Díaz Piedra, G. Olay Fuentes, R. Hernández Gómez, D. Cervantes-Villagrana, J. Presno-Beral, L.E. Alcántara Gómez, Determinación de los intervalos de referencia de biometría hemática en población mexicana, Rev. Lat. Patol. Clin. 59 (2012) 243–250.
[50] Oruganti T., Petrova E., Oraevsky A.A., Ermilov S.A. Speed of sound and acoustic attenuation of compounds affected during optoacoustic monitoring of thermal therapies measured in the temperature range from 5°C to 60°C. In: Oraevsky AA, Wang L V., editors. Proc. SPIE. Photons Plus Ultrasound Imaging Sens. 2015., 2015, p. 1–9. https://doi.org/10.1117/12.2083375.
[51] G. Gopala Krishna, A.K.W. Anwar Ali, A. Ahmad, Absorption of ultrasound in human blood, C2-311-C2-314, Le. J. Phys. Colloq. 51 (1990), https://doi.org/10.1051/jphyscol:1990275.
[52] E.L. Bradley, J. Sacerio, The velocity of ultrasound in human blood under varying physiologic parameters, J. Surg. Res 12 (1972) 290–297, https://doi.org/10.1016/0022-4804(72)90024-8.
[53] E.J. Kanfer, B.A. Nicol, Haemoglobin concentration and erythrocyte sedimentation rate in primary care patients, J. R. Soc. Med 90 (1997) 16–18, https://doi.org/10.1177/014107689709000106.
[54] A. Zhbanov, S. Yang, Effects of aggregation on blood sedimentation and conductivity, PLoS One 10 (2015) 1–25, https://doi.org/10.1371/journal.pone.0129337.
[55] T. Feng, Y. Zhu, R. Morris, K.M. Kozloff, X. Wang, The feasibility study of the transmission mode photoacoustic measurement of human calcaneus bone in vivo, Photoacoustics 23 (2021) 100273, https://doi.org/10.1016/j.pacs.2021.100273.
[56] G. Xu, Z.-X. Meng, J.D. Lin, J. Yuan, P.L. Carson, B. Joshi, et al., The Functional Pitch of an Organ: Quantification of Tissue Texture with Photoacoustic Spectrum Analysis, Radiology 271 (2014) 248–254, https://doi.org/10.1148/radiol.13130777.
[57] G. Xu, J.B. Fowlkes, C. Tao, X. Liu, X. Wang, Photoacoustic Spectrum Analysis for Microstructure Characterization in Biological Tissue: Analytical Model, Ultrasound Med Biol. 41 (2015) 1473–1480, https://doi.org/10.1016/j.ultrasmedbio.2015.01.010.
[58] N. Rathi, S. Sinha, B. Chinni, V. Dogra, N. Rao, Feasibility of quantitative tissue characterization using novel parameters extracted from photoacoustic power spectrum, Biomed. Signal Process Control 57 (2020) 101719, https://doi.org/10.1016/j.bspc.2019.101719.
[59] W. Xie, T. Feng, M. Zhang, J. Li, D. Ta, L. Cheng, et al., Wavelet transform-based photoacoustic time-frequency spectral analysis for bone assessment, Photoacoustics 22 (2021) 100259, https://doi.org/10.1016/j.pacs.2021.100259.
[60] W. Strober, Trypan Blue Exclusion Test of Cell Viability, A3.B.1-A3.B.3, Curr. Protoc. Immunol. 111 (2015), https://doi.org/10.1002/0471142735.ima03bs111.
[61] S. Mahmoodkalayeh, H.Z. Jooya, A. Hariri, Y. Zhou, Q. Xu, M.A. Ansari, et al., Low Temperature-Mediated Enhancement of Photoacoustic Imaging Depth, Sci. Rep. 8 (2018) 4873, https://doi.org/10.1038/s41598-018-22898-2.
[62] W.G. Murphy, The sex difference in haemoglobin levels in adults - Mechanisms, causes, and consequences, Blood Rev. 28 (2014) 41–47, https://doi.org/10.1016/j.blre.2013.12.003.
[63] E.M. Strohm, M.J. Moore, M.C. Kolios, Single Cell Photoacoustic Microscopy: A Review, IEEE J. Sel. Top. Quantum Electron 22 (2016) 137–151, https://doi.org/10.1109/JSTQE.2015.2497323.
[64] J.de Paz and Vivanco F. El fenomeno del apilamiento de los eritrocitos. Rev Clin Española 1955;LVI:73–87.
[65] S. Chen, B. Gavich, S. Zhnag, Y. Mahler, S. Yedgar, Monitoring of erythrocyte aggregate morphology under flow by computerized image analysis, Biorheology 32 (1995) 487–496, https://doi.org/10.1016/0006-355x(95)91988-f.
[66] T. Winsor, G.E. Burch, Rate of Sedimentation of Erythrocytess in Sickle Cell Anemia, Arch. Intern Med 73 (1944) 41–52, https://doi.org/10.1001/archinte.1944.00210130049007.
[67] K. Jan, S. Usami, J. A.Smith, Influence of oxygen tension and hematocrit reading on ESRs of sickle cells. Role of RBC aggregation, Arch. Intern Med 141 (1981) 1815–1818, https://doi.org/10.1001/archinte.141.13.1815.
[68] L.W. Diggs, J. Bibb, The erythrocyte in sickle cell anemia, J. Am. Med Assoc. 112 (1939) 695, https://doi.org/10.1001/jama.1939.02800080015004.
[69] J. Tripette, T. Alexy, M.D. Hardy-Dessources, D. Mougenel, E. Beltan, T. Chalabi, et al., Red blood cell aggregation, aggregate strength and oxygen transport potential of blood are abnormal in both homozygous sickle cell anemia and sickle-hemoglobin C disease, Haematologica 94 (2009) 1060–1065, https://doi.org/10.3324/haematol.2008.005371.
[70] A. Pérez-Pacheco, R.G. Ramírez-Chavarría, R.M. Quispe-Siccha, M.P. Colín-García, Dynamic modeling of photoacoustic sensor data to classify human blood samples, Med Biol. Eng. Comput. (2023), https://doi.org/10.1007/s11517-023-02939-3.

Argelia Pérez-Pacheco is a Researcher in Medical Sciences and the current coordinator of the Research and Technological Development Unit (UIDT) at the Hospital General de México. She received her Ph.D. in Materials Science and Engineering in 2009 and a B.S. degree in physics in 2003 from the National Autonomous University of Mexico (UNAM). She has carried out 5 postdoctoral stays in different laboratories. Her main scientific interest is in the biophotonic area, focusing on biomedical and photoacoustic applications. She has more than 20 years of teaching. She is a member of the National System of Researchers in Mexico.

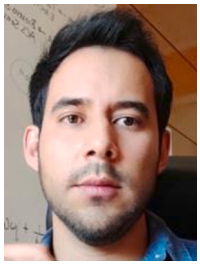

Roberto G. Ramírez-Chavarría. He received a B.Sc. degree in computer science engineering and a Ph.D. degree in electrical engineering, from the Universidad Nacional Autónoma de México (UNAM), in 2019. Afterward, he held a Postdoctoral position at Instituto de Ingeniería, UNAM (II-UNAM), working in the design and development of sensors and biosensors. He has been a Visitant Researcher at Vrije Universiteit Brussel (Belgium), KTH Royal Institute of Technology (Sweden), and Grenoble INP (France). Currently, he is an Assistant Professor at Electro-Mechanics Department at IIUNAM. His research interests include biosensors and bioelectronics, smart sensors, instrumentation, and signal processing. Currently, he is a member of the National System of Researchers in Mexico.

Marco Polo Colín-García received his B.S. degree in Physics from the National Autonomous University of Mexico, in Mexico City, and his M.Sc. degree in Engineering. Currently, he is a Ph. D. student at the Institute of Applied Sciences and Technology (ICAT) at the same university. His research interests focus on Photoacoustic Tomography modality applied to biological samples.

Flor del Carmen Cortés Ortegón holds a degree in Physics from the Faculty of Science UNAM and a Master's degree in Engineering from the National Autonomous University of Mexico (UNAM). She is currently a Ph.D. student in Engineering at UNAM in the biomedical device department group of ICAT-UNAM. She has also contributed to research in Photoacoustic at the research and technological development unit (UIDT) of the General Hospital of Mexico, Dr. Eduardo Liceaga.

Rosa María Quispe-Siccha received a B.Sc. degree in Physics at the National University of Trujillo, Perú in 2003, and a direct Ph.D. in Materials Science and Engineering with an honorable mention at the National Autonomous University of Mexico (UNAM) in 2009. Three Postdoctoral stays at the UNAM, Mexico. Since 2013 she has been a Researcher in Medical Sciences "C" in the Research and Technological Development Unit (UIDT) of the General Hospital of Mexico "Dr. Eduardo Liceaga". She was the coordinator of the UIDT (2013–16). She is a researcher in medical physicist with ten years of experience in detecting and analyzing pathological and non-pathological tissue bio-signals using the non-invasive pulsed photoacoustic technique. And the synthesizing/characterization of biopolymers for tissue simulators.

Adolfo Martinez Tovar. He did postgraduate studies in the Department of Molecular Biology of CINVESTAV-IPN. Currently is a researcher at the Hematology Service of the General Hospital of Mexico "Dr. Eduardo Liceaga". His research lines focus on the study of the oncogenes responsible for drug resistance as well as the immunological mechanisms that cause the development of leukemia. Currently, he has more than 60 articles published in international journals as well as training more than 20 graduate students from different postgraduate courses. He is a professor of the university course specializing in hematology.

Irma Olarte-Carrillo. Biologist graduated from UNAM, interested in hematological research. She graduated with a Master's degree and a Ph.D. in biological sciences also at UNAM. Currently, she works in basic hematological research at the Hospital General de Mexico, whose principal projects are focused on the association of tumor genes and the prognostic clinical implication in patients with oncohematological disorders and molecular mechanisms related to resistance to chemotherapeutic agents.

Luis Polo-Parada received his Ph. D. in Neurosciences from Case Western Reserve University. He is an Associate Professor in the Department of Medical Pharmacology and Physiology and Resident Investigator at the Dalton Cardiovascular Research Center at the University of Missouri. Doctor Polo-Parada is responsible for teaching Neurosciences to first-year medical Students and is responsible for several online undergraduate and graduate level courses. His research interests include electrophysiology, heart development, Nanomedicine, diverse aspects of Instrumentation, nanomaterials in biology and medicine, and photoacoustics.

Gerardo Gutiérrez-Juárez was born in Cuautapehual, Puebla. He received his Ph. D degree in physics from CINVESTAV, Mexico City, México, in 1998. He has been a Full Time Professor with the University of Guanajuato Campus Leon, León los Aldama, México, since 1998, and a regular Visiting Scholar with Dalton Cardiovascular Research Center, University of Missouri Columbia, MO, USA. His research interests focus on laser-induced ultrasound, photoacoustic detection of cells, and numerical approaches to photoacoustic signal detection.